THE ASTROPHYSICAL JOURNAL, 455:L59–L62, 1995 December 10

EVIDENCE FOR THERMAL ABSORPTION INSIDE CASSIOPEIA A

N. E. KASSIM,[1] R. A. PERLEY,[2] K. S. DWARAKANATH,[3] AND W. C. ERICKSON[4]
Received 1995 June 26; accepted 1995 September 12

ABSTRACT

Subarcminute resolution images of Cas A at 74 and 333 MHz are presented. Comparison with each other and with higher frequency observations indicates that the spectral index of its nonthermal emission flattens below 333 MHz and that the effect is confined toward the central 1′ of the source and is maximum at its center. The source of the flattening is unknown, although we show that the data are consistent with absorption by ionized gas inside the radio shell. Such a component may be related to unshocked ejecta still freely expanding within the boundaries of the reverse shock as delineated by X-ray observations.

Subject headings: ISM: individual (Cassiopeia A) — radio continuum: ISM — supernovae: general — supernova remnants

1. INTRODUCTION

Low-frequency (<1 GHz) radio observations provide a unique means for investigating supernova remnants (SNRs) and their interaction with the interstellar medium (ISM). These nonthermal sources are brighter at long wavelengths, and, together with higher frequency measurements, these data provide a sensitive measure of their radio spectrum. Since their radio spectral indices are related to the energy spectrum of the synchrotron-emitting electrons, they provide information on the shock acceleration processes operating in SNRs (Reynolds & Ellison 1992; Chevalier 1990; Ellison et al. 1994). The lowest frequency measurements (<100 MHz) also provide information on the ISM along the line of sight toward SNRs since they are sensitive to absorption processes by intervening ionized gas (Vinyaikin et al. 1987; Dulk & Slee 1972, 1975; Kassim 1989a, b). Unfortunately, these studies have been limited by the poor angular resolution available to the few instruments operating at the longest wavelengths.

To address this deficiency, we have used the VLA's[5] (Napier, Thompson, & Ekers, 1983) subarcminute resolution 74 and 333 MHz observing systems to map Cas A at higher angular resolution than previously possible. We present 74 and 333 MHz images of Cas A, which are combined with previously obtained 1381 MHz VLA data (Braun 1987; Braun, Gull, & Perley 1987; Anderson et al. 1991; Anderson & Rudnick 1995 hereafter AR95) to generate spectral index maps. These reveal a prominent and unexpected region of spectral index flattening toward the center of the source.

The large, arcminute-scale size of the flatter spectrum region suggests that it may not be related to the smaller, arcsecond-scale radio spectral index variations reported by Anderson et al. (1991) and AR95. The latter are believed to be related to the shock acceleration processes associated with the blast wave and its interaction with the circumstellar environment of the progenitor star. While the effect we measure might be related to these or other unknown processes, we find that absorption by thermal gas inside the radio-emitting shell can readily account for our observations, and we note that theory predicts a natural property of young, shell-type SNRs which could plausibly explain it.

Our radio observations are summarized in § 2 and the results presented in § 3. We discuss these results in § 4, and our conclusions are summarized in § 5.

2. OBSERVATIONS

Cas A was observed simultaneously at 74 MHz (eight antennas available) and 333 MHz (27 antennas available) at the VLA from 1991 August to 1993 July. The observations consist of snapshots obtained during the A (two epochs), B (two epochs), and C (one epoch) configurations, resulting in an integration time of ~5 hr. The angular resolution was ~25″ at 74 MHz and 6″ at 333 MHz. The largest scale structure the images are sensitive to is ~90′ at 74 MHz and ~30′ at 333 MHz. Figure 1 shows a plot of visibility (u, v) coverage obtained for Cas A at 74 MHz.

The data were reduced utilizing the technique of ionospheric phase referencing as described by Kassim et al. (1993), in order to remove the effects of ionospheric phase variations and increase the coherence time.

The continuum images of Cas A, each convolved with a circular beam of 25″ (HPBW), are shown in Figures 2*a*–2*b* (Plates L5) (74 MHz) and Figures 3*a*–3*b* (Plate L6) (333 MHz). We also obtained the VLA data of Braun et al. (1987) and Anderson et al. (1991) at 1381 MHz and imaged it to the same 25″ resolution as shown in Figures 4*a*–4*b* (Plate L7).

The absolute flux density scale was set by normalizing the integrated flux density of Cas A to the epoch 1965.0 values of Baars et al. (1977) ($S^{74\ \mathrm{MHz}} = 22{,}885$ Jy, $S^{333\ \mathrm{MHz}} = 7625$ Jy, $S^{1381\ \mathrm{MHz}} = 2472$ Jy). This was done in order to avoid correcting data taken at separate epochs for Cas A's time-dependent spectrum (Shklovsky 1969), for which details are controversial (Erickson & Perley 1975; Reese 1990; Hook, Duffett-Smith, & Shakeshaft 1992). This procedure could introduce offsets in integrated flux density between images since the reconstructed flux differs somewhat from the adopted values. However, this could not impact the main result of this Letter—the flattening

[1] Code 7213, Naval Research Laboratory, Washington, DC 20375-5351; nkassim@shimmer.nrl.navy.mil.
[2] National Radio Astronomy Observatory, P.O. Box 0, Socorro, NM 87801; rperley@nrao.edu.
[3] Raman Research Institute, C. V. Raman Avenue, Sadashivanagar P.O., Bangalore 560 080; dwaraka@rri.ernet.in.
[4] Physics Department, University of Tasmania, G.P.O. 252C, Hobart, Tasmania 7001; wce@astro.umd.edu.
[5] The Very Large Array is a facility of the National Radio Astronomy Observatory, operated by Associated Universities, Inc., under contract with the National Science Foundation.

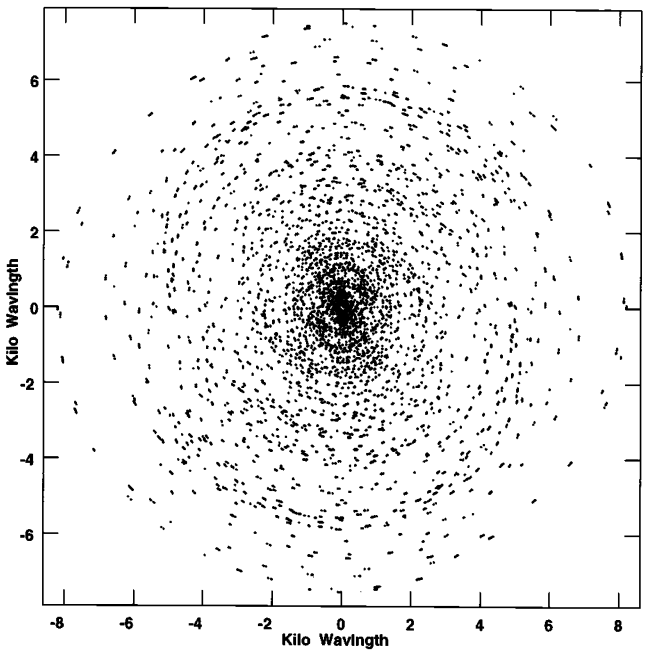

FIG. 1.—Visibility (u vs. v) plot of the 74 MHz data set. Data were obtained from two consecutive VLA configuration cycles in order to increase the visibility coverage provided by the eight antennas outfitted with 74 MHz dipoles. During the second configuration campaign the 74 MHz antennas were placed at different physical locations than for the first configuration campaign. Only one out of every 10 visibility points is actually plotted.

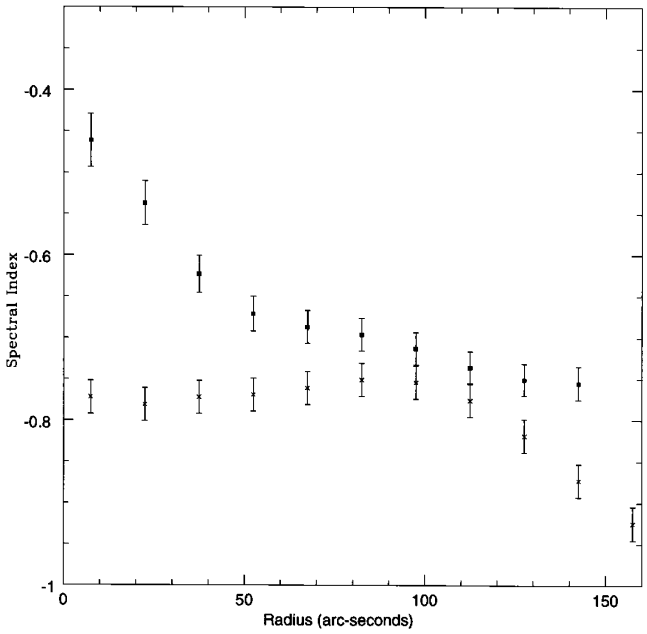

FIG. 8.—Plot of spectral index as a function of radius between 74 and 333 MHz (*filled squares*) and 333 and 1381 MHz (*crosses*). The plotted points are average values within concentric annuli of width and separation 15″. Error bars are 1 σ uncertainties based on the rms errors in the flux density maps added in quadrature with the quoted 2% uncertainty in the Baars et al. (1976) spectrum of Cas A, then propagated through to the spectral index calculation. $R = 0''$ was defined at the geometric center of Cas A's bright radio ring as determined from higher resolution radio studies (Rudnick 1995).

of the spectrum toward the center of the source below 333 MHz, as described in § 3, since integrated flux normalization offsets cannot introduce spectral index gradients.

3. RESULTS

Figures 2–4 and comparison with higher frequency radio maps show that the arcminute-scale features of Cas A's brightness distribution are unchanged over a wide frequency range and show the limb-brightened morphology typical of shell-type Galactic SNRs.

Figures 5–7 (Plates L8–L10) are spectral index maps made between 333 and 1381 MHz (hereafter the PL spectral index image), 74 and 333 MHz (4P), and 74 and 1381 MHz (4L), respectively. Hereafter we define the geometric center of Cas A ($R = 0$) at $\alpha = 23^{h}21^{m}10\overset{s}{.}5$, $\delta = 58°32'20\overset{''}{.}6$ as determined from higher frequency studies of the broad radio ring (Rudnick 1995). The PL map (Figs. 5*a*–5*b*) indicates a roughly constant spectral index of roughly -0.77 ± 0.05 within $R < 100''$, with the exception of a region of steeper spectrum emission to the immediate southwest of the center that is discussed further below. Beyond $R > 100''$ the map shows a gradual steepening in spectral index as a function of radius. The 4P (Figs. 6*a*–6*b*) and 4L (Figs. 7*a*–7*b*) images are consistent with the PL image for the regions beyond $\sim R > 80''$, but both show a pronounced flattening in the spectral index that increases radially inward from $R \sim 1'$ and reaches a maximum near $R \sim 0$. The deviation from the average shell spectrum of roughly $\sim$0.77, hereafter $\Delta\alpha$, reaches a maximum of about $+0.3$ and about $+0.2$ at the centers of the 4P and 4L spectral index images, respectively. This trend is consistent with an absorption mechanism acting below 333 MHz, as discussed further below. All these trends are better illustrated in Figure 8, where we have plotted the ring-averaged spectral index as a function of radius for concentric annuli of width and separation 15″ from the 4P and PL spectral index maps.

We performed a variety of tests with different mapping parameters; while some of the details varied, the flattening at the center was always strongly present, so we are confident that it is real. As a further check, we followed the "forced VTESS" robustness test utilized by AR95 in their 6 and 20 cm studies of Cas A. This meant using our 333 MHz image, which was made using a standard Fourier transform of the measured visibility data followed by a conventional CLEAN (i.e., AIPS task "MX"), as a default model for a maximum entropy-based imaging (i.e., AIPS task VTESS) of our 74 MHz data. A new spectral index map between the 74 MHz "forced VTESS" map and the 333 MHz image nicely reproduced the basic features seen in Figures 6*a*–6*b*.

We note from Figure 8 that both the 4P and PL spectral index data indicate a gradual steepening beyond Cas A's bright radio ring located at $\sim R = 100''$. This is especially pronounced in the PL curve of Figure 8, which can be extended further than the 4P curve because of superior S/N. AR95 have found evidence for a radial trend in knot spectral index, with flatter spectrum knots residing preferentially in the radio ring, while a spectrally steeper population of knots resides beyond this. This result is consistent with our measurements and suggests that the diffuse emission may exhibit the same radial trend in spectral index as the compact features. According to AR95, the spectral index of compact features is not determined by current acceleration processes but is influenced by the history of particle acceleration in the environment through which they currently move. Accordingly, our results suggest that the same

environmental factors that influence the spectra of the compact features may also affect the diffuse emission.

We note also that an extended region of steeper spectrum emission seen best in Figure 5 and located near $\alpha = 23^h21^m08^s$, $\delta = 58°32'$ matches extremely well in both position and morphology with a population of steeper spectrum knots seen on the higher frequency spectral index maps of AR95. Keohane, Rudnick, & Anderson (1996) attribute this feature to a collision with a dense external cloud. This feature also appears on the 4P and 4L spectral index maps (Figs. 6 and 7), but less prominently since there the effect "competes" with the spectral index flattening effect that dominates the central regions of those maps.

4. DISCUSSION

4.1. *Likely Sources of Absorption*

Here we consider absorption mechanisms that could suppress radio emission toward the center of SNRs. The high brightness temperatures and magnetic field strengths required for quenching by either synchrotron self-absorption or the Razin-Tsitovich effect are not present in Cas A, nor could either of these mechanisms or a break in the energy spectrum of the relativistic electrons below 333 MHz account for the observed, centrally concentrated geometry of the flattening.

This leads us to consider free-free absorption by ionized gas. This can take three forms: (1) absorption by either a distributed or discrete ionized component of the ISM along the line of sight to the source, (2) absorption by an ionized component either surrounding or mixed with the synchrotron-emitting electrons within the SNR shell, or (3) absorption by an ionized component interior to the limb-brightened radio shell and reverse shock.

Absorption by form (1) has been argued by Vinyaikin et al. (1987), who favor van den Bergh's (1971) suggestion of a relic ionized halo left over from the SN explosion in order to explain the observed low-frequency turnover of the continuum spectrum below 20 MHz. However, for a $T_e = 10{,}000$ K gas, the optical depths calculated based on either the optical data (Peimbert 1971; Peimbert & van den Bergh 1971), with $\tau_{74\ \mathrm{MHz}} = 0.05$, or the radio data (Vinyaikin et al. 1987), giving $\tau_{74\ \mathrm{MHz}} = 0.02$, are far too low to account for the measured spectral index variations presented here, nor would they be consistent with the observed, centrally condensed morphology of the flattening. Also, while Kassim (1989a, b) has shown that absorption by a likely H II–related component of the ISM can produce low-frequency absorption along the line of sight to SNRs, this mechanism is also ruled out for Cas A by the observed, centrally condensed morphology of the spectral index anomaly. Such would also be the case for form (2), absorption by an ionized component mixed within the shell of the relativistically emitting electrons.

Last we consider absorption by an ionized component interior to the radio shell. Let us consider free-free absorption from an ionized sphere of radius $R_i \sim 1'$, which at Cas A's distance of 2.8 kpc (van den Bergh 1971) is ~0.8 pc. If the emission from the front and back synchrotron-emitting faces of the radio shell are equal, then we can express the optical depth τ toward the center of the ionized sphere to the apparent spectral index gradient $\Delta\alpha$ by

$$\tau = -\ln\left[2(10^{(a*\Delta\alpha\,-\,0.5)})\right],$$

where $a \equiv \log(\nu_{\mathrm{low}}/\nu_{\mathrm{high}})$. This gives $\tau_{74\ \mathrm{MHz}} \sim 1.3$ for $\Delta\alpha \sim +0.3$ from the center of the 4P spectral index map. The free-free optical depth τ is related to the emission measure EM (cm^{-6} pc), observing frequency ν (MHz), and electron temperature T_e (K) by

$$\tau = 1.643 \times 10^5\ \nu^{-2.1}\ \mathrm{EM}\ T_e^{-1.35},$$

where EM is defined as

$$\mathrm{EM} = \int n_e^2\, dl,$$

and where n_e is the thermal electron density in cm^{-3} and the integral is taken along a line of sight to the source. Thus, we can estimate EM for the presumed thermal gas (for $\tau_{74\ \mathrm{MHz}} = 1.3$) by

$$\mathrm{EM} = 750\ \mathrm{cm}^{-6}\ \mathrm{pc}\left(\frac{T_e}{1000\ \mathrm{K}}\right)^{1.35}.$$

While this gas would become rapidly optically thick at lower frequencies, only ~10% of the total radio emission would be affected since the presumed absorbing gas does not cover the bright limb or the front face. (The ring outside a radius of ~1′ accounts for ~75% of the total radio flux.) Thus, it is unlikely that such an absorbing component is related to the observed lower frequency turnover in the continuum spectrum below 20 MHz.

4.2. *Comparison with Theory*

Theory suggests that cool ($T_e \sim 1000$ K), unshocked ejecta interior to the reverse shock in young SNRs like Cas A may be related to the apparent absorption suggested by our observations. If the region of spectral index flattening we observe within the central ~1′ was produced by free-free absorption from such unshocked material, it would be expected to lie interior to the reverse shock. This is consistent with X-ray observations which place the reverse shock in Cas A at $R \leqq 120''$ (Lozinskaya 1992 and references therein). Furthermore, $R = 1'$ corresponds to unshocked ejecta at an expansion velocity of $\sim 3 \times 10^3$ km s^{-1} based on Cas A's distance and age. Chevalier & Liang (1989) (taking $n = 9$ in their eq. [2.1] and assuming the total energy and mass in the SN explosion to be 10^{51} ergs and 5–10 $M_\odot$, respectively) have shown that this is also approximately where the radial density profiles for models of SN ejecta makes a transition from flat to steep power laws. Thus, any hypothesized low-frequency thermal absorption beyond $R = 1'$ should decrease rapidly since little unshocked material extends beyond this radius. Therefore, the observed geometry is consistent with absorption by ionized, unshocked ejecta located interior to the reverse shock.

A highly model dependent estimate of the mass of ionized gas (M_i) within a presumed sphere of radius $R_i \sim 1'$ (as inferred from our measured value of the optical depth) is

$$M_i \sim 19\ M_\odot \left(\frac{R_i}{1'}\right)^{2.5} \left(\frac{T_e}{1000\ \mathrm{K}}\right)^{0.7}$$

for pure O II. This is large and shows that more sophisticated modeling is required. Unfortunately, few models exist for the ionization structure of unshocked ejecta inside reverse shocks, with SN 1006 being the only case where direct evidence for this gas has been found (Hamilton & Sarazin 1984a, b; Hamilton & Fesen 1988).

4.3. *Suggestions for Future Observations*

Lower frequency (<74 MHz) observations are desired to establish the frequency dependence of the spectral index flattening we detect toward the center of Cas A and to search for this effect in other young SNRs. If the effect was due to absorption by hot ($T_e \sim 10{,}000$ K) ionized gas inside the source, it might be detected optically. However, with a visual extinction $A \sim 4.3$ (Searle 1971; van den Bergh, Marscher, & Terzian 1973), the apparent EM inferred from our data would be diluted by a factor ~100 to values ≤100 cm^{-6} pc. If the gas consists of processed ejecta such as oxygen or its nuclear burning by-products, its equilibrium temperature would be lower, and hence its emission measure (at fixed optical depth) would be much lower. In this case, a search for hyperfine transitions in the far-infrared may be warranted. Finally, if pervaded by a magnetic field, polarization measurements may be able to detect the depolarizing or Faraday rotation effects of any ionized gas interior to the source at radio wavelengths.

5. SUMMARY

We have presented subarcminute-resolution VLA images of Cas A at 74 and 333 MHz. Comparison with higher frequency data indicates that the spectral index of its nonthermal emission flattens below 333 MHz and that the effect is confined toward the central 1′ of the source and is maximum at its center. The source of the flattening is unknown, although we show that the data are consistent with absorption by ionized gas inside the radio shell. Such a component may be related to unshocked ejecta still freely expanding within the boundaries of the reverse shock as delineated by X-ray observations.

Finally, we see evidence for a radial trend of steepening spectral index in the region beyond the bright radio ring similar to the radial trend in the knot spectral index reported by AR95 and which may be related to the particle acceleration properties of the SNR.

The authors thank R. Chevalier and C. Sarazin for useful discussions about unshocked ejecta in SNRs and L. Rudnick for making available his 1381 MHz image of Cas A and for important comments on the spectral index analysis. Basic research in radio and infrared astronomy at the Naval Research Laboratory is supported by the Office of Naval Research.

REFERENCES

Anderson, M., & Rudnick, L. 1995, ApJ, in press (AR95)
Anderson, M., Rudnick, L., Leppik, P., Perley, R. A., & Braun, R. 1991, ApJ, 373, 146
Baars, J. W. M., Genzel, R., Pauliny-Toth, I. I. K., & Witzel, A. 1977, A&A, 61, 99
Braun, R. 1987, A&A, 171, 233
Braun, R., Gull, S. F., & Perley, R. A. 1987, Nature, 327, 395
Chevalier, R. A. 1990, in Lecture Notes in Physics, ed. Low-Frequency Astrophysics from Space, N. E. Kassim & K. W. Weiler (Heidelberg: Springer), 362, 130
Chevalier, R. A., & Liang, E. P. 1989, ApJ, 344, 332
Dulk, G. A., & Slee, O. B. 1972, Australian, J. Phys., 25, 429
———. 1975, ApJ, 199, 61
Ellison, D. C., et al. 1994, PASP, 106, 780
Erickson, W. C., & Perley, R. A. 1975, ApJ, 200, L83
Hamilton, A. J. S., & Fesen, R. A. 1988, ApJ, 327, 178
Hamilton, A. J. S., & Sarazin, C. L. 1984a, ApJ, 281, 682
———. 1984b, ApJ, 287, 282
Hook, I. M., Duffett-Smith, P. J., & Shakeshaft, J. R. 1992, A&A, 255, 285
Kassim, N. E. 1989a, ApJ, 347, 915
———. 1989b, ApJS, 71, 799
Kassim, N. E., Perley, R. A., Erickson, W. C., & Dwarakanath, K. S. 1993, AJ, 106, 2218
Keohane, J., Rudnick, L., & Anderson, M. C. 1996, ApJ, submitted
Lozinskaya, T. A. 1992, Supernovae and Stellar Winds in the Interstellar Medium (New York: AIP)
Napier, P. J., Thompson, A. R., & Ekers, R. D. 1983, Proc. IEEE, 71, 1295
Peimbert, M. 1971, ApJ, 170, 261
Peimbert, M., & van den Bergh, S. 1971, ApJ, 167, 223
Rees, N. 1990, MNRAS, 243, 637
Reynolds, S. P., & Ellison, D. C. 1992, ApJ, 399, L75
Rudnick, L. 1995, private communication
Searle, L. 1971, ApJ, 168, 41
Shklovsky, I. S. 1960, USSR–AJ, 4, 355
van den Bergh, S. 1971, ApJ, 165, 259
van den Bergh, S., Marscher, A. P., & Terzian, Y. 1973, ApJS, 26, 19
Vinyaikin, E. N., Nikonov, V. A., Tarasov, A. F., Tokarev, Y. V., & Yurishchev, M. A. 1987, Soviet Astron.–AJ, 31, 517

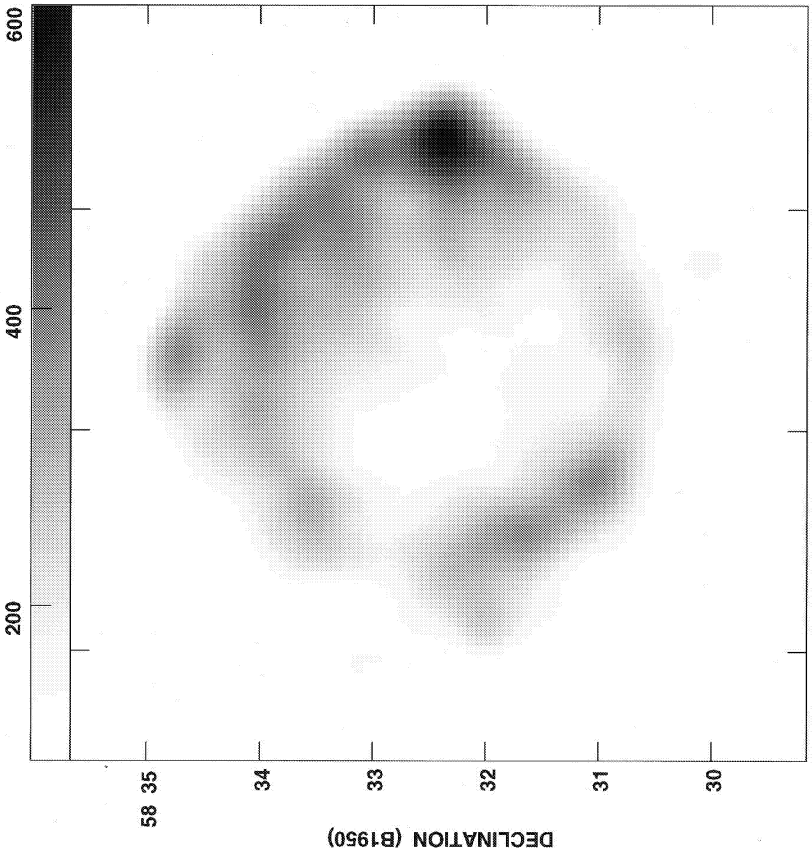

FIG. 2b

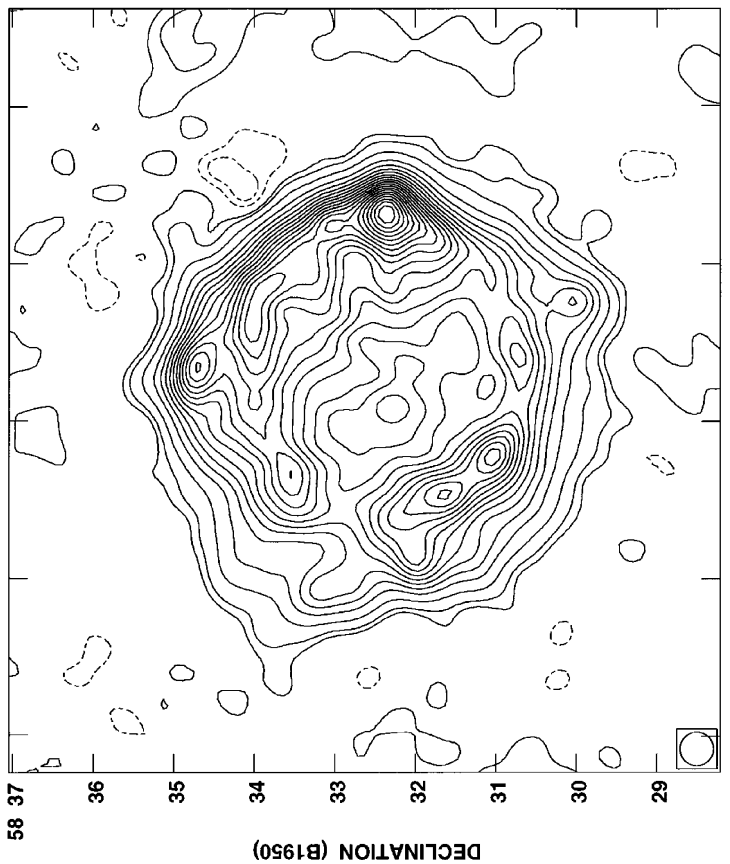

FIG. 2a

FIG. 2.—Contour (*a*) and gray-scale (*b*) flux density plots of the SNR Cas A at 74 MHz. The peak brightness temperature is 598 Jy beam^{-1}, and the rms noise σ is ~6 Jy beam^{-1}. The angular resolution is 25″ and is shown at the lower left. Contours in (*a*) are at (−2, −1, 1, 2, 5, 10, 15, 20, 25, 30, 35, 40, 45, 50, 55, 60, 65, 70, 75, 80, 85, 90, 95, 100) σ. For (*b*) the gray-scale flux density range is from 100 to 600 Jy beam^{-1} as indicated by the scale at the top of the image.

KASSIM et al. (see 455, L59)

PLATE L6

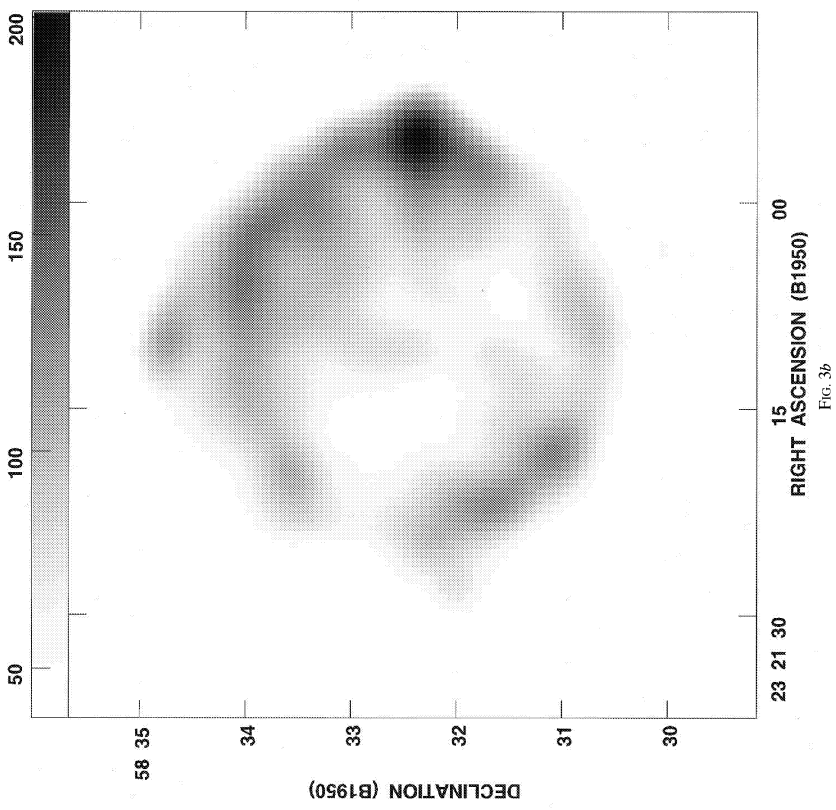

FIG. 3b

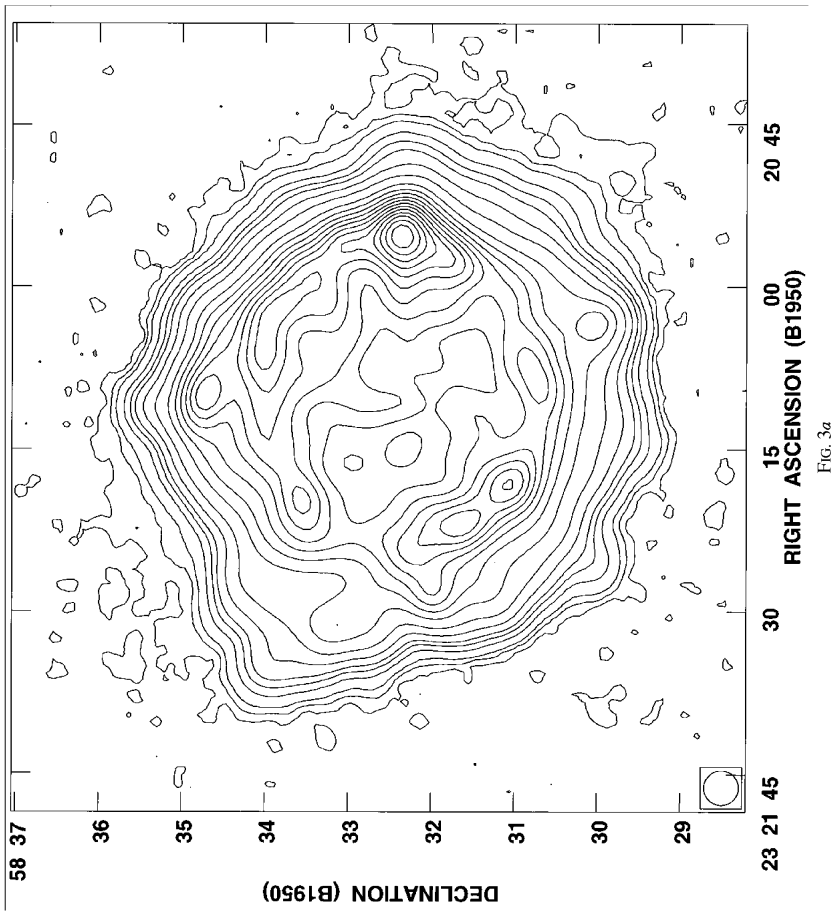

FIG. 3a

FIG. 3.—Contour (*a*) and gray-scale (*b*) flux density plots of the SNR Cas A at 333 MHz. The peak brightness temperature is 195 Jy beam^{-1}, and the rms noise σ is ~35 mJy beam^{-1}. The angular resolution is 25″ and is shown at the lower left. Contours in (*a*) are at (−2, 2, 5, 10, 30, 60, 100, 200, 400, 800, 1200, 1600, 2000, 2400, 2800, 3200, 3600, 4000, 4400, 4800, 5200, 5600) σ. For (*b*) the gray-scale flux density range is from 40 to 200 Jy beam^{-1}, as indicated by the scale at the top of the image.

KASSIM et al. (see 455, L59)

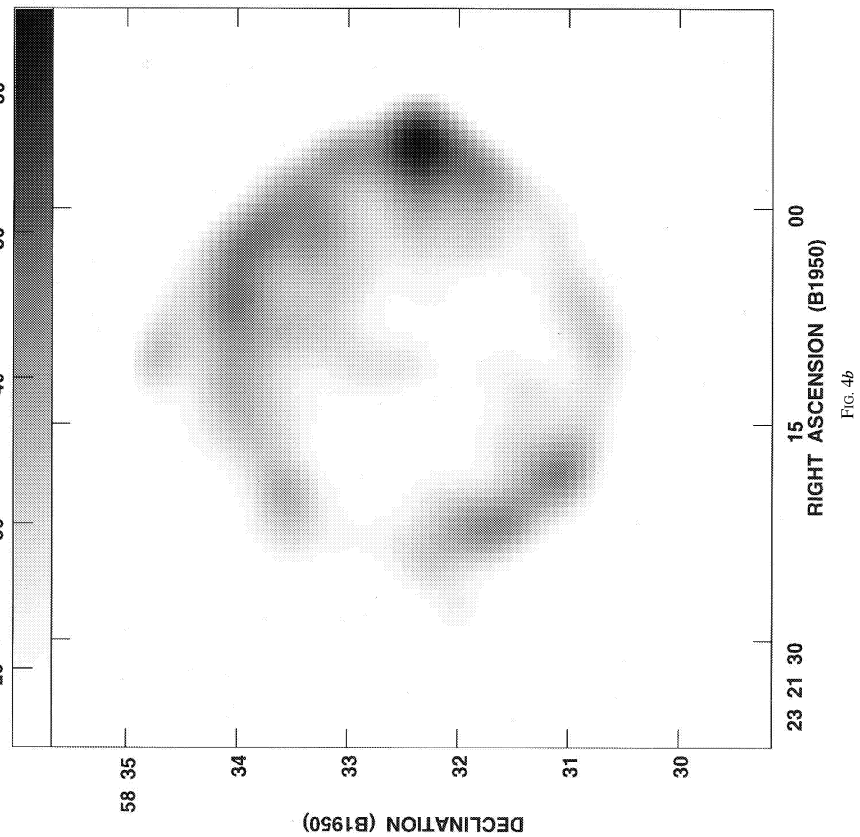

FIG. 4a

FIG. 4b

FIG. 4.—Contour (*a*) and gray-scale (*b*) flux density plots of the SNR Cas A at 1381 MHz, courtesy of L. Rudnick. The peak brightness temperature is 63.2 Jy beam^{-1}, and the rms noise σ is ~135 mJy beam^{-1}. The angular resolution is 25″ and is shown at the lower left. Contours in (*a*) are at (−3, −3, 6, 20, 50, 80, 110, 140, 170, 200, 230, 260, 290, 320, 350, 380, 410, 440) σ. For (*b*) the gray-scale flux density range is from 15 to 65 Jy beam^{-1}, as indicated by the scale at the top of the image.

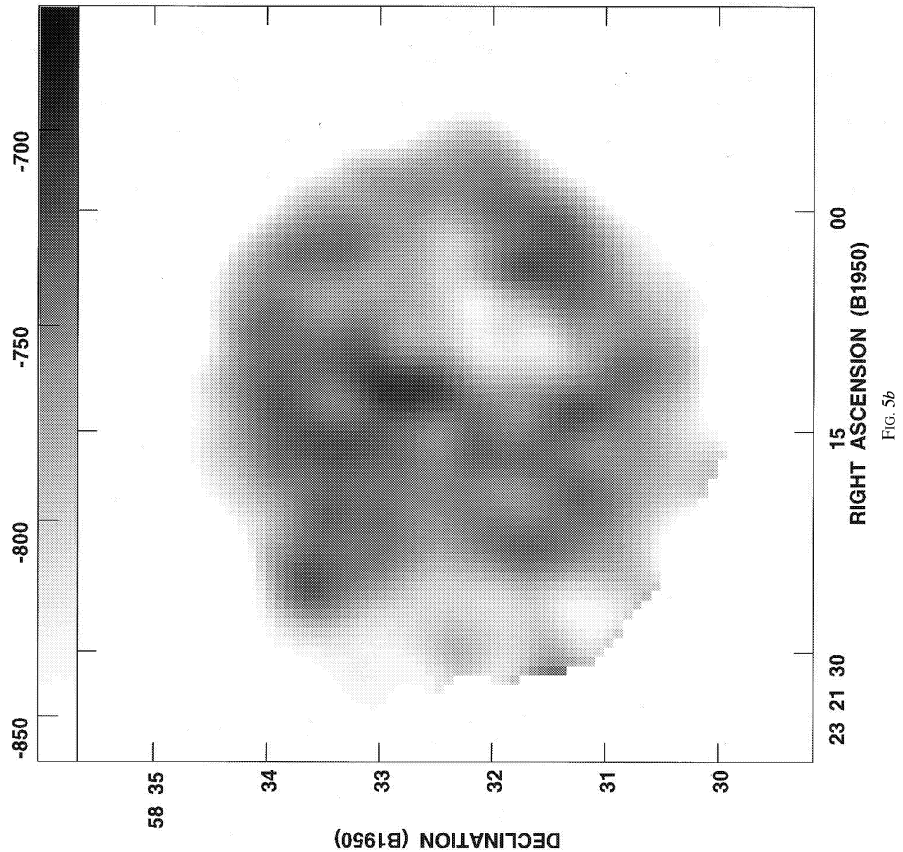

FIG. 5b

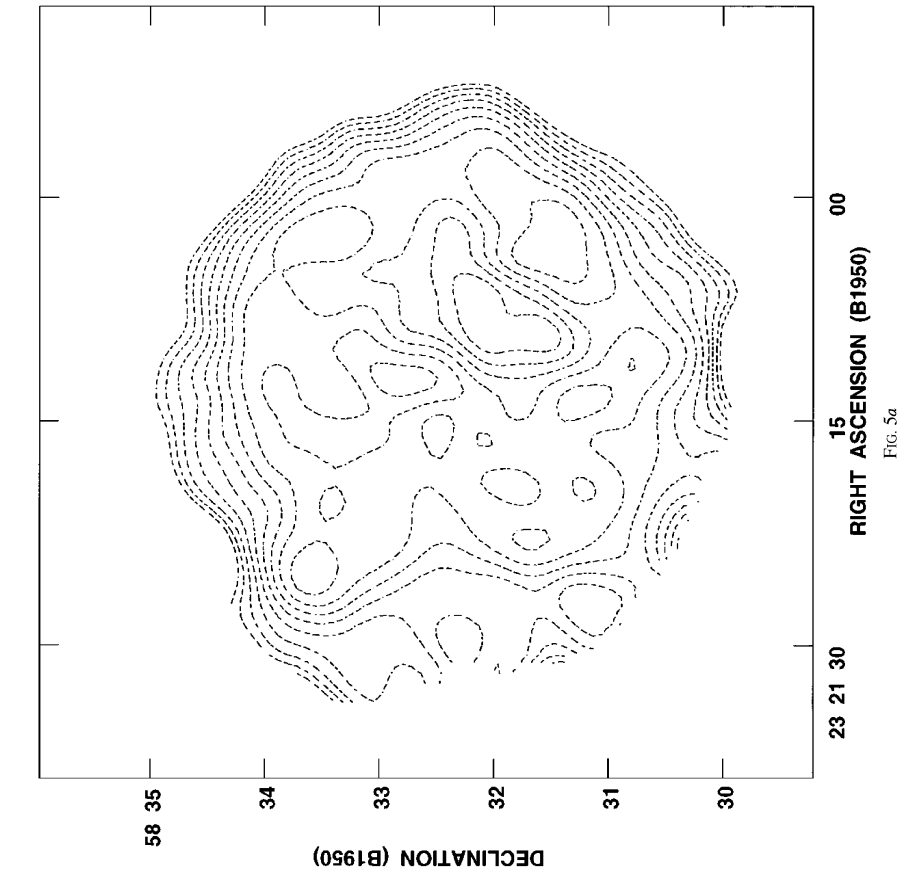

FIG. 5a

FIG. 5.—Contour (*a*) and gray-scale (*b*) spectral index maps of the SNR Cas A between 333 and 1381 MHz. The peak value of the map is −1.146, and the contours are at (−9, −8.8, −8.6, −8.4, −8.2, −8, −7.8, −7.6, −7.4, −7.2, −7, −6.8, −6.6, −6.4) times 0.1 in units of spectral index ($S \propto \nu^{-\alpha}$). This image was made from the images shown in Figs. 3 and 4 above. For (*b*) the gray-scale range in spectral index is from −860 to −670 in units of spectral index times 10^{-3}, as indicated by the scale at the top of the image.

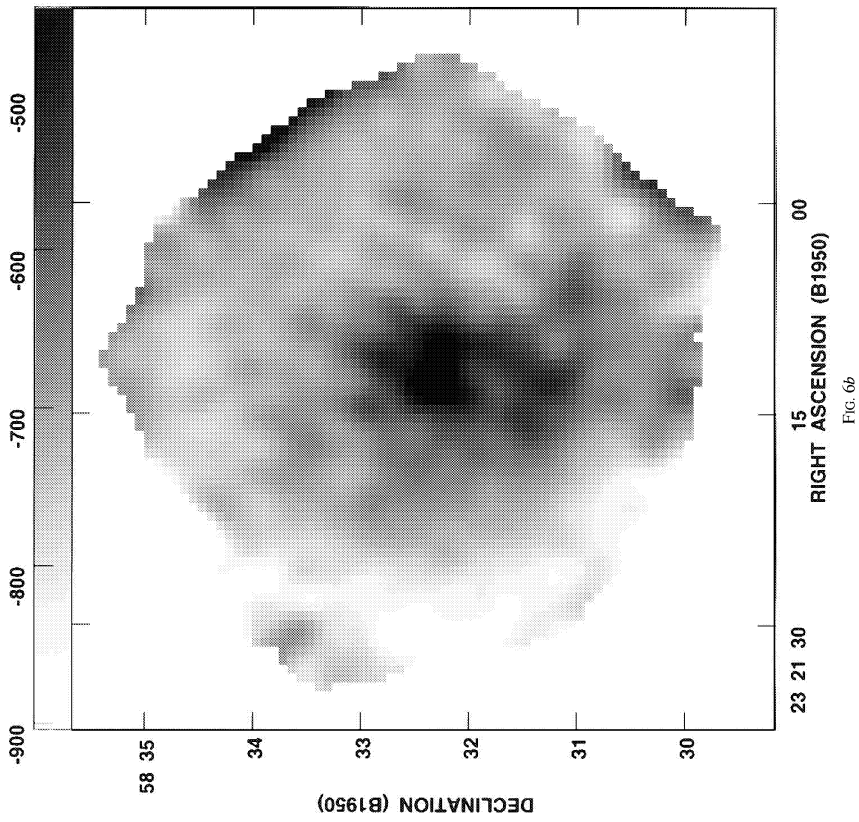

FIG. 6b

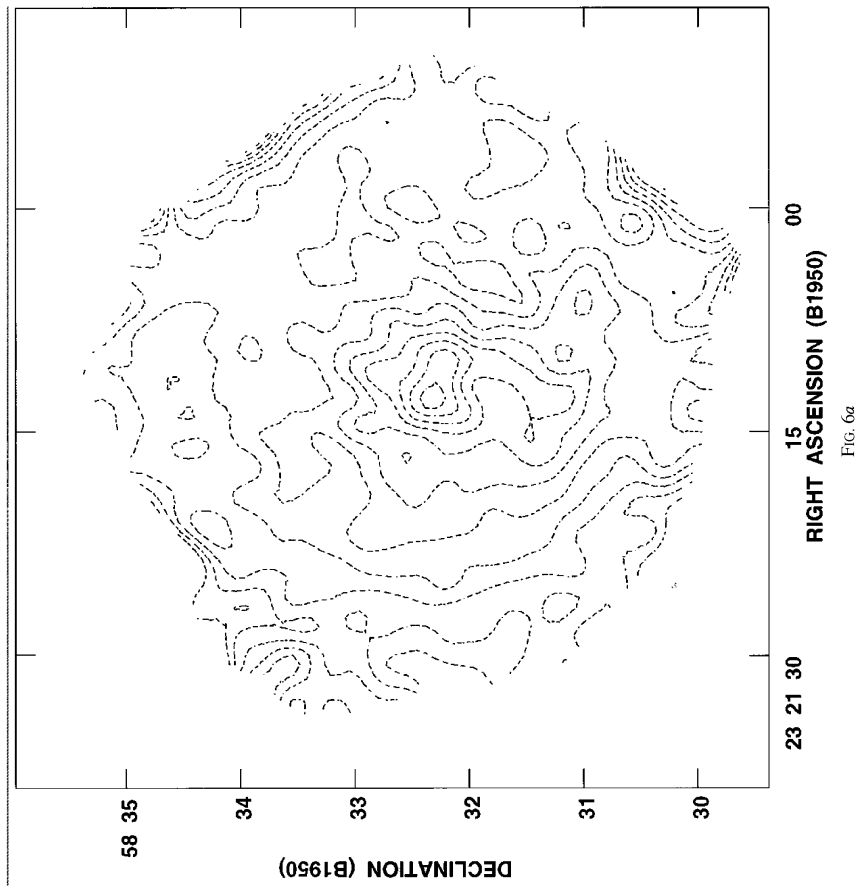

FIG. 6a

FIG. 6.—Contour (*a*) and gray-scale (*b*) spectral index maps of the SNR Cas A between 74 and 333 MHz. The peak value of the map is −1.08, and for (*a*) the contours are at (−18, −17, −16, −15, −14, −13, −12, −11, −10, −9, −8) times 0.05 in units of spectral index ($S \propto \nu^{-\alpha}$). This image was made from the images shown in Figs. 2 and 3 above. For (*b*) the gray-scale range in spectral index is from −900 to −450 in units of spectral index times 10^{-3}, as indicated by the scale at the top of the image.

PLATE L10

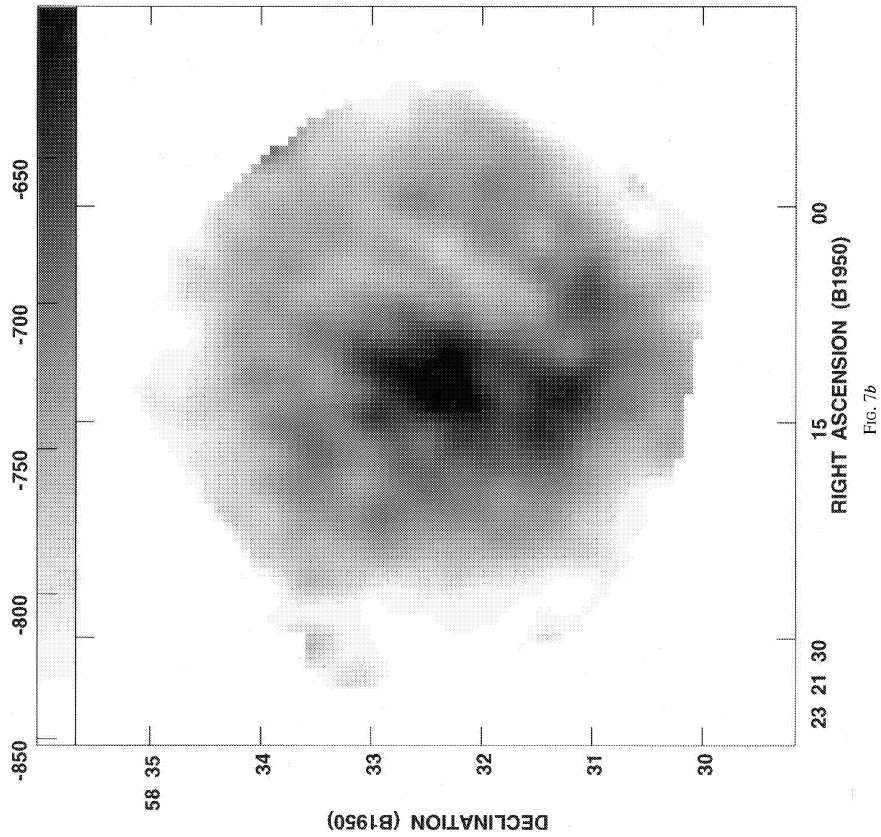

FIG. 7b

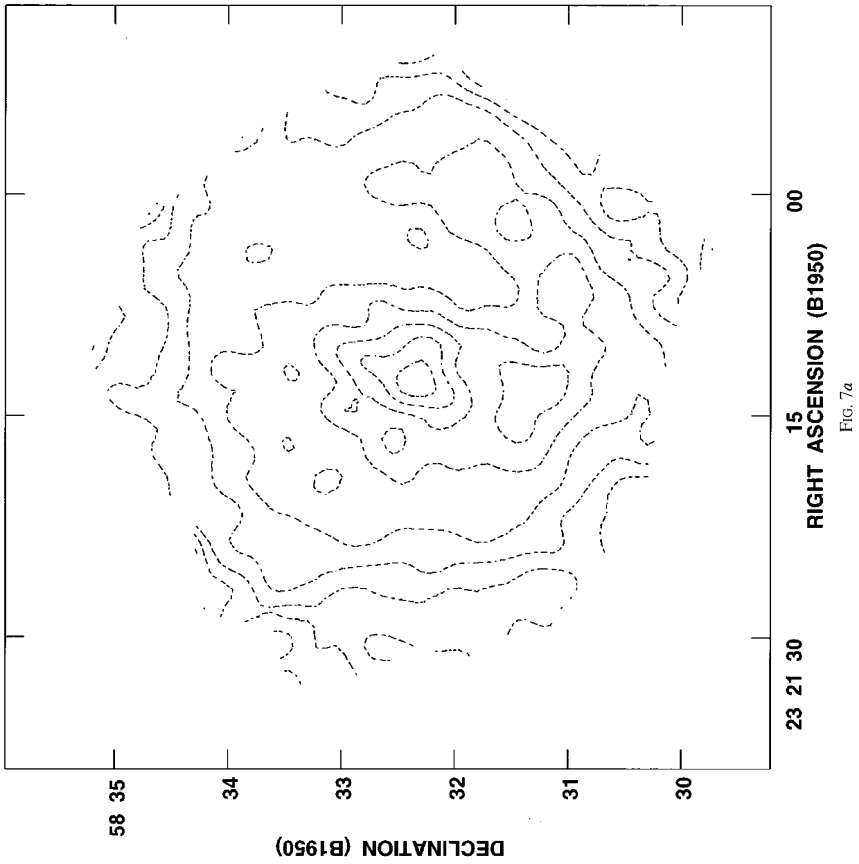

FIG. 7a

FIG. 7.—Contour (*a*) and gray-scale (*b*) spectral index maps of the SNR Cas A between 74 and 1381 MHz. The peak value of the map is −0.913, and for (*a*) the contours are at (−9.0, −8.6, −8.2, −7.8, −7.4, −7.0, −6.6, −6.2, −5.8, −5.4) times 0.1 in units of spectral index ($S \propto \nu^{-\alpha}$). This image was made from the images shown in Figs. 2 and 4 above. For (*b*), the gray-scale range in spectral index is from −850 to −600 in units of spectral index times 10^{-3}, as indicated by the scale at the top of the image.